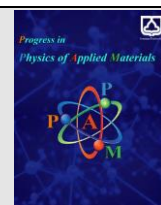# Physical Properties of Electrode Materials of Rechargeable Lithium Ion Batteries via DFT Calculations

Zeinab Saeedi pour[a], Jaafar Jalilian[b], S. H. Reza Shojaei[a],*

[a] Department of Physics, Faculty of Science, Sahand University of Technology, Tabriz, P.O. Box: 513351996, Iran.
[b] Department of Physics, Faculty of Science, Yasouj University, Yasouj, P.O. Box: 7591874934, Iran.

ARTICLE INFO

ABSTRACT

We performed a density functional theory (DFT) study on Li_2VO_2F to assess its electronic structure. All calculations were conducted employing the plane wave pseudopotentials basis set. Electronic structure of Li_2VO_2F was calculated in the framework of the Hubbard U density functional theory (DFT+U) method. The geometry of the unit cell was optimized in triclinic and monoclinic phases. The effect of adding the Hubbard parameter on the band structure as well as the partial density of states were investigated and the contribution of different atoms in the total density of states was investigated separately. Hubbard parameter added the electron-electron interaction in the calculations, which has led to an increase in the bandgap value and more accurate results compared to the existing experimental results. It was observed that the monoclinic phase exhibits a smaller gap bandwidth than the triclinic phase. Also the calculated band structure indicates the presence of an indirect gap in both phases of this compound.

1. Introduction

Energy storage devices play a pivotal role in portable electronics and stable energy facilities [1]. Among these devices, lithium-ion batteries stand out as the most promising type due to their high energy density, extended lifespan, and broad applicability [2, 3]. Presently, lithium-ion batteries are the technology of choice for portable electronic devices. However, meeting the demanding requirements of high energy density and power in extensive applications, such as hybrid or electric vehicles, continues to pose a significant challenge.

The primary factor limiting the energy density of lithium-ion batteries is the cathode. The specific capacity of current-generation Li-ion cathodes (150–200 mAh/g) and next-generation cathodes (200–250 mAh/g) falls significantly short compared to that of current-generation carbon anodes (250–350 mAh/g) and next-generation anodes like Si (>1000 mAh/g) [4].

Furthermore, the working voltage of lithium-ion batteries is affected by the cathode material. The cathode material must endure numerous cycles without structure collapse. There is a research to explore new cathode materials for Li-ion batteries that offer a superior energy density, utilizing elements that are more abundant, cost-effective, and less hazardous than the conventional Co-based materials [5].

A common issue with cobalt-based lithium-ion battery cathodes is their toxicity, flammability, low capacity, and relatively high cost. Consequently, ongoing research aims to replace these cathodes with materials that offer high energy density, affordability, and reduced toxicity [6].

Li-rich disordered rock salt (DRS) materials show a good potential to be used as high-capacity cathodes for Li-ion batteries. These materials represent a promising alternative as they can cycle reversibly more than one lithium ion per transition metal (TM), making them highly attractive for this purpose [7-9]. These materials display face-centered cubic rock salt structures where oxygen and fluorine anions stack in a face-centered cubic arrangement, with transition metal and lithium cations randomly occupying octahedral

---

interstitial sites. Replacing some oxygen atoms with fluorine induces a lower oxidation state of the TM, enhancing the lithium content and, consequently, energy density [10-12].

Initially, DRS structures were thought to possess a totally random distribution of cations and anions. However, recent findings indicate that certain structures among these can display localized atomic arrangements or short-range ordering (SRO).

An exemplary material in this category is Li-rich DRS Li_2VO_2F, introduced by Chen's group [8]. This innovative cathode material boasts a 1.8 Li^+ capacity per TM, equivalent to 420 mAh/g (compared to 280 mAh/g for the standard $LiCoO_2$ electrode), at an average potential of 2.5 V versus Li^+/Li.

Nevertheless, the Li_2VO_2F cathode has been observed to suffer from irreversible degradation reactions and experience a decline in capacity over time [13, 14]. To address these instabilities, a better understanding of the structure properties of the material during battery operation is crucial.
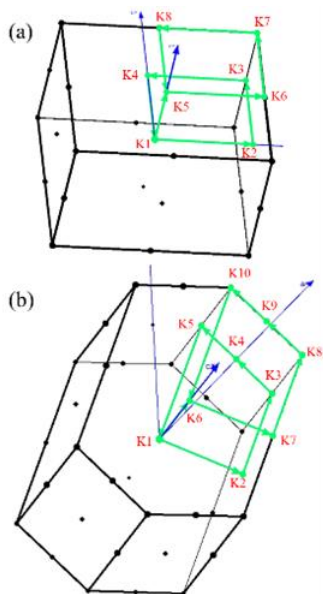
Fig. 1. Schematic crystal structure representations of Li_2VO_2F disordered structure in monoclinic (a) and triclinic (b) phases.

A recent discovery shows that an SRO cation exists in multiple DRS substances, affecting transport properties and electrochemical efficiency significantly [15-18].

Although traditional XRD methods fall short in revealing this short-range ordering, alternative experimental studies such as NMR [16-18], X-ray spectro-microscopy [17], and electron diffraction [15] confirm its existence. However, in fluorine-substituted DRS materials, aside from NMR, no experimental method has successfully characterized anionic sites.

To our knowledge, no study has explored the electronic properties of Li_2VO_2F. In this research, we will investigate the band structure and density of states of this compound.

2. Computational Details

All calculations in this study were conducted using density functional theory [19, 20], employing the plane wave pseudopotentials basis set within the Quantum Espresso computing package [19]. Given that the

crystalline form of Li_2VO_2F has been reported in both monoclinic and triclinic phases, we optimized the geometry of the Li_2VO_2F unit cell in both phases using DFT to identify the most stable geometric structure in terms of interatomic forces. Total energy and other properties were calculated using the Perdew–Burke–Ernzerhof (PBE) model and the Generalized Gradient Approximation theory (GGA) [20].

A cut-off energy equivalent to 70 Rydbergs and a k-point meshing of 12x12x12 symmetry points were selected to ensure the convergence of the total energy for the structure's unit cell within a 3 milli-Rydbergs range. To account for the electron correlation of localized d electrons, we applied a simplified form of the DFT+U approximation introduced by Dodaro [21]. It is noteworthy that the results of the GGA+U approximation are contingent on the chosen value of the U parameter, which itself depends on the valence state of the transition metal ion and the crystal structure. However, this dependence is generally not substantial, and a change in Hubbard's parameter by 0.5 V influences the lithium entry potential by only 0.1 V [22].

Considering the Hubbard parameter in DFT simulations is crucial as it predicts electron localization with remarkable precision, preventing the incorrect prediction of metallic conductivity in insulating systems [23].

In systems with strong electron interaction, utilizing the Hubbard model can yield more realistic outcomes. Broadly, increasing the Hubbard U parameter implies enhancing electron-electron interaction via the mean-field approximation [24].

In some studies, the value of U is chosen to align the obtained results with experimental data (energy gap, lithium entry potential, etc.). In other studies, the value of U is determined through initial studies [25]. In this research, the Hubbard U parameter for the vanadium atom V is set at 4.25. It is assumed that the value of U remains consistent for both pure and lithium incorporated systems.

3. Results and discussion

The unit cell geometry was optimized in both triclinic and monoclinic structures. While there is relatively good agreement between the calculated parameters and experimental data [4, 8, 26], these results are generally overestimated compared to existing experimental results, a characteristic property of the Generalized Gradient Approximation (GGA) [27], which accounts for exchange and correlation effects in DFT.

Despite this overestimation, the difference with experimental cell parameters falls within the standard accuracy range of this method.

Electronic bands related to the triclinic and monoclinic phases are depicted in Figures 2 and 3. In the monoclinic phase, the maximum of the valence band is located at the symmetry points k_5 and k_9, while the minimum of the conduction band is located at the point k_6, and the energy gap value calculated in this phase is also 2.2181 eV. In the triclinic phase, the maximum of the valence band is located between the symmetry points k_3 and k_4, while the minimum of the conduction band is located between the symmetry points k_7 and k_8. The energy gap value calculated in this phase is also 2.2301 eV.

By increasing the Hubbard U parameter to 4.25 eV, there is an observable increase in the band gap value in the band structure of Li_2VO_2F, aligning more closely with experimental results. Results obtained from calculations without considering the Hubbard parameter differ by a few electron volts from experimental results, underscoring the dominance of electron-electron interaction in the Li_2VO_2F system [22].

Therefore, results from calculations without considering the Hubbard parameter are not presented in this report.

The width of the band gap was also extracted using density of states diagrams. The triclinic band gap is slightly smaller than the monoclinic band gap, suggesting higher electron transfer capacity in the triclinic phase and better conductivity compared to the monoclinic phase.
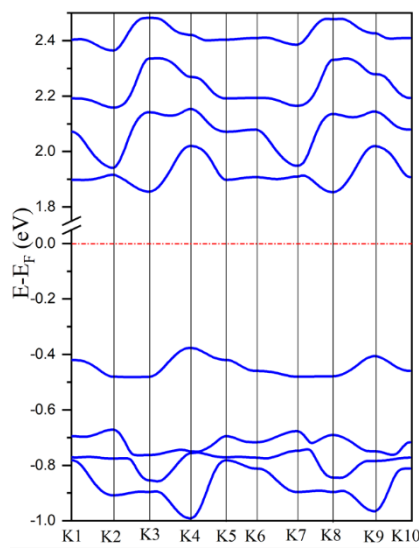

Fig. 2. Band structure of Li_2VO_2F in triclinic phase.

According to the band structure obtained in the triclinic Li_2VO_2F phase, this structure is semiconducting with an indirect gap.
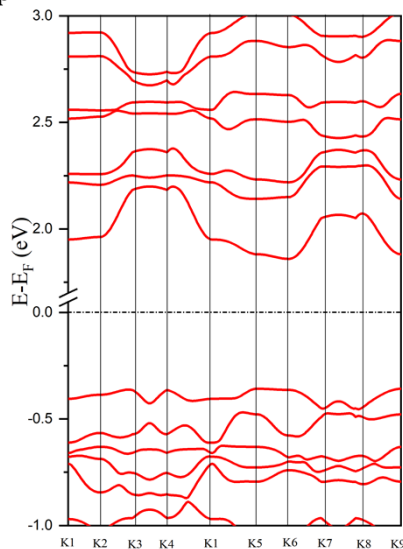

Fig. 3. Band structure of Li_2VO_2F in monoclinic phase.

According to the band structure obtained in the monoclinic phase of Li_2VO_2F, this structure is semiconducting and has an indirect gap.

In the band structure diagrams for Li_2VO_2F in both triclinic and monoclinic phases, the Fermi energy level is positioned at zero on the energy axis.

In the study of the partial density of states of Li_2VO_2F, we see that in the monoclinic phase, the observed density of states, in the ranges greater than the Fermi energy, i.e. [1.5, 6 eV], is the result of the participation of Li, V and O atoms.

Actually, V atoms have the most effect in the range of [1.5, 5 eV]. While in the range of [5, 6 eV], the dominant effect is related to the Li atoms.

In the ranges lower than the Fermi energy, all three Li, V and O atoms have significant peaks in the range of [-0.5, -1.5 eV] and [-3, -6 eV].

F atom participates in the density of states only in an interval relatively far from the gap, i.e. [-3.5, -6 eV], and has significant peaks.
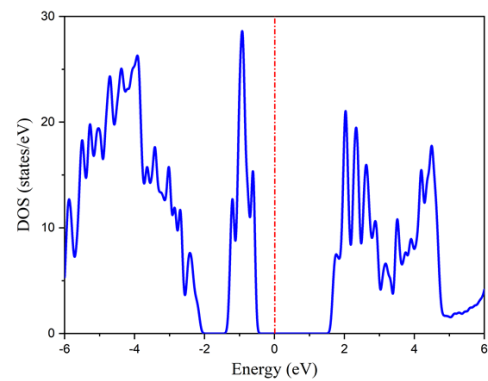

Fig. 4. Density of states of Li_2VO_2F in monoclinic phase.

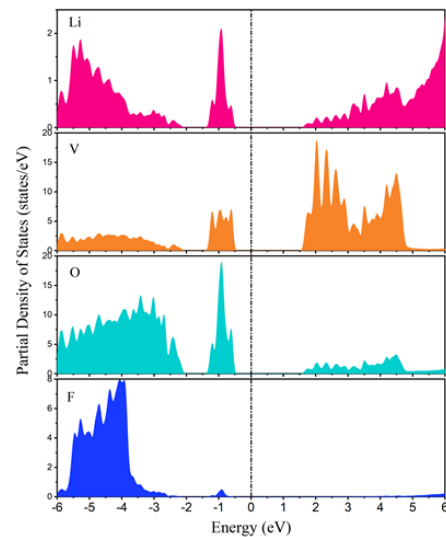**Fig. 5.** Partial density of states of Li_2VO_2F in monoclinic phase.
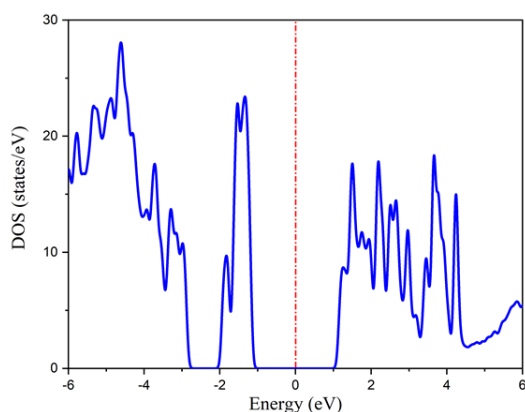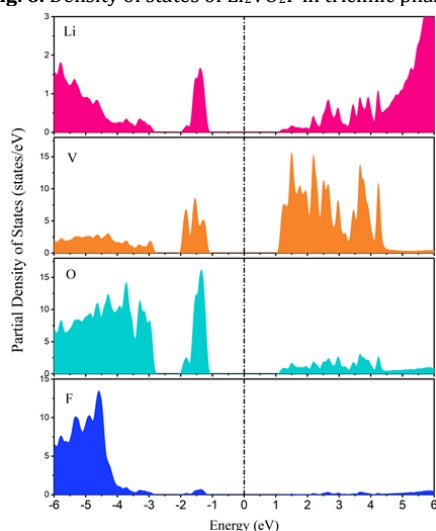
Fig. 6. Density of states of Li_2VO_2F in triclinic phase.

Fig. 7. Partial density of states of Li2VO2F in the triclinic phase.

In the triclinic phase, the participation rate of the orbitals is relatively similar to the monoclinic phase. The only difference is that, in the monoclinic phase, the Fermi level is nearer to the valence band. While in the triclinic phase, the Fermi level is exactly in the middle of the gap.

Also, the height of the peaks close to the Fermi level in the triclinic phase is slightly higher than monoclinic phase, which indicates the greater participation of orbitals in this phase.

4. Conclusion

In this study, the GGA+U method was utilized to calculate the band structure of Li_2VO_2F in different monoclinic and triclinic phases using Quantum Espresso and Nanolab software packages. According to the authors, no similar work has been published on this compound, and there are very few experimental studies available. In this research, by adding the Hubbard parameter, we included the electron-electron interaction in the calculations, which has led to an increase in the bandgap value and more accurate results compared to the existing experimental results.

The calculated band structure indicates the presence of an indirect gap in both monoclinic and triclinic phases of this compound. The monoclinic phase exhibits a smaller band gap width than the triclinic phase. Due to the positions of CBM and VBM in these two phases, it is expected that electron transfer in the monoclinic phase is

accompanied by the exchange of phonons with higher momentum compared to the triclinic phase.

Conflicts of Interest

The author declares that there is no conflict of interest regarding the publication of this article.

References

[1] Goodenough, J.B. and Kim, Y., 2010. Challenges for rechargeable Li batteries. *Chemistry of materials*, *22*(3), pp.587-603.

[2] Schmuch, R., Wagner, R., Hörpel, G., Placke, T. and Winter, M., 2018. Performance and cost of materials for lithium-based rechargeable automotive batteries. *Nature energy*, *3*(4), pp.267-278.

[3] Zhang, H., Eshetu, G.G., Judez, X., Li, C., Rodriguez-Martínez, L.M. and Armand, M., 2018. Electrolyte additives for lithium metal anodes and rechargeable lithium metal batteries: progress and perspectives. *Angewandte Chemie International Edition*, *57*(46), pp.15002-15027.

[4] Wang, X., Huang, Y., Ji, D., Omenya, F., Karki, K., Sallis, S., Piper, L.F., Wiaderek, K.M., Chapman, K.W., Chernova, N.A. and Whittingham, M.S., 2017. Structure evolution and thermal stability of high-energy-density Li-ion battery cathode Li_2VO_2F. *Journal of The Electrochemical Society*, *164*(7), p.A1552.

[5] Mozhzhukhina, N., Kullgren, J., Baur, C., Gustafsson, O., Brant, W.R., Fichtner, M. and Brandell, D., 2020. Short-range ordering in the Li-rich disordered rock salt cathode material Li_2VO_2F revealed by Raman spectroscopy. *Journal of Raman Spectroscopy*, *51*(10), pp.2095-2101.

[6] Nitta, N., Wu, F., Lee, J.T. and Yushin, G., 2015. Li-ion battery materials: present and future. *Materials today*, *18*(5), pp.252-264.

[7] Clément, R.J., Lun, Z. and Ceder, G., 2020. Cation-disordered rocksalt transition metal oxides and oxyfluorides for high energy lithium-ion cathodes. *Energy & Environmental Science*, *13*(2), pp.345-373.

[8] Chen, R., Ren, S., Knapp, M., Wang, D., Witter, R., Fichtner, M. and Hahn, H., 2015. Disordered lithium-rich oxyfluoride as a stable host for enhanced Li^+ intercalation storage. *Advanced Energy Materials*, *5*(9), p.1401814.

[9] Cambaz, M.A., Vinayan, B.P., Euchner, H., Johnsen, R.E., Guda, A.A., Mazilkin, A., Rusalev, Y.V., Trigub, A.L., Gross, A. and Fichtner, M., 2018. Design of nickel-based cation-disordered rock-salt oxides: The effect of transition metal (M= V, Ti, Zr) substitution in $LiNi_{0.5}M_{0.5}O_2$ binary systems. *ACS applied materials & interfaces*, *10*(26), pp.21957-21964.

[10] Chen, R., Ren, S., Yavuz, M., Guda, A.A., Shapovalov, V., Witter, R., Fichtner, M. and Hahn, H., 2015. Li^+ intercalation in isostructural Li_2VO_3 and Li_2VO_2 F with

O^{2-} and mixed O^{2-}/F^- anions. *Physical Chemistry Chemical Physics*, *17*(26), pp.17288-17295.

[11] Pereira, N., Badway, F., Wartelsky, M., Gunn, S. and Amatucci, G.G., 2009. Iron oxyfluorides as high capacity cathode materials for lithium batteries. *Journal of the Electrochemical Society*, *156*(6), p.A407.

[12] Choi, W. and Manthiram, A., 2006. Superior capacity retention spinel oxyfluoride cathodes for lithium-ion batteries. *Electrochemical and solid-state letters*, *9*(5), p.A245.

[13] Källquist, I., Naylor, A.J., Baur, C., Chable, J., Kullgren, J., Fichtner, M., Edstrom, K., Brandell, D. and Hahlin, M., 2019. Degradation mechanisms in Li_2VO_2F Li-rich disordered rock-salt cathodes. *Chemistry of Materials*, *31*(16), pp.6084-6096.

[14] Baur, C., Källquist, I., Chable, J., Chang, J.H., Johnsen, R.E., Ruiz-Zepeda, F., Mba, J.M.A., Naylor, A.J., Garcia-Lastra, J.M., Vegge, T. and Klein, F., 2019. Improved cycling stability in high-capacity Li-rich vanadium containing disordered rock salt oxyfluoride cathodes. *Journal of Materials Chemistry A*, *7*(37), pp.21244-21253.

[15] Kwon, D.H., Lee, J., Artrith, N., Kim, H., Wu, L., Lun, Z., Tian, Y., Zhu, Y. and Ceder, G., 2020. The impact of surface structure transformations on the performance of Li-excess cation-disordered rocksalt cathodes. *Cell Reports Physical Science*, *1*(9).

[16] Clément, R.J., Kitchaev, D., Lee, J. and Ceder, G., 2018. Short-range order and unusual modes of nickel redox in a fluorine-substituted disordered rocksalt oxide lithium-ion cathode. *Chemistry of Materials*, *30*(19), pp.6945-6956.

[17] Kan, W.H., Deng, B., Xu, Y., Shukla, A.K., Bo, T., Zhang, S., Liu, J., Pianetta, P., Wang, B.T., Liu, Y. and Chen, G., 2018. Understanding the effect of local short-range ordering on lithium diffusion in $Li_{1.3}Nb_{0.3}Mn_{0.4}O_2$ single-crystal cathode. *Chem*, *4*(9), pp.2108-2123.

[18] Jones, M.A., Reeves, P.J., Seymour, I.D., Cliffe, M.J., Dutton, S.E. and Grey, C.P., 2019. Short-range ordering in a battery electrode, the 'cation-disordered'rocksalt $Li_{1.25}Nb_{0.25}Mn_{0.5}O_2$. *Chemical Communications*, *55*(61), pp.9027-9030.

[19] Hohenberg, P. and Kohn, W., 1964. Inhomogeneous electron gas. *Physical review*, *136*(3B), p.B864.

[20] Kohn, W. and Sham, L.J., 1965. Self-consistent equations including exchange and correlation effects. *Physical review*, *140*(4A), p.A1133.

[21] Giannozzi, P., Baroni, S., Bonini, N., Calandra, M., Car, R., Cavazzoni, C., Ceresoli, D., Chiarotti, G.L., Coccoccioni, M., Dabo, I. and Dal Corso, A., 2009. QUANTUM ESPRESSO: a modular and open-source software project for quantum simulations of materials. *Journal of physics: Condensed matter*, *21*(39), p.395502.

[22] Giorgi, G., Fujisawa, J.I., Segawa, H. and Yamashita, K., 2013. Small photocarrier effective masses featuring ambipolar transport in methylammonium lead iodide perovskite: a density functional analysis. *The journal of physical chemistry letters*, *4*(24), pp.4213-4216.

[23] Dudarev, S.L., Botton, G.A., Savrasov, S.Y., Humphreys, C.J. and Sutton, A.P., 1998. Electron-energy-loss spectra and the structural stability of nickel oxide: An $LSDA^+ U$ study. *Physical Review B*, *57*(3), p.1505.

[24] Sgroi, M.F., Lazzaroni, R., Beljonne, D. and Pullini, D., 2017. Doping $LiMnPO_4$ with cobalt and nickel: a first principle study. *Batteries*, *3*(2), p.11.

[25] Fronzi, M., Assadi, M.H.N. and Hanaor, D.A., 2019. Theoretical insights into the hydrophobicity of low index CeO_2 surfaces. *Applied Surface Science*, *478*, pp.68-74.

[26] Aikebaier, F., 2014. Effects of electron-electron interaction in pristine and doped graphene.

[27] Cococcioni, M. and De Gironcoli, S., 2005. Linear response approach to the calculation of the effective interaction parameters in the LDA+U method. *Physical Review B*, *71*(3), p.035105.

[28] Ren, S., Chen, R., Maawad, E., Dolotko, O., Guda, A.A., Shapovalov, V., Wang, D., Hahn, H. and Fichtner, M., 2015. Improved voltage and cycling for Li^+ intercalation in high-capacity disordered oxyfluoride cathodes. *Advanced science*, *2*(10), p.1500128.

[29] Haas, P., Tran, F. and Blaha, P., 2009. Calculation of the lattice constant of solids with semilocal functionals. *Physical Review B*, *79*(8), p.085104.